# Forward-scattering ring structure and the spectra dependence on laser frequency

Å. Lindberg and B. Ståhlberg
*Accelerator Laboratory, Department of Physics, University of Helsinki, P.O. Box 43, FIN-00014 Helsinki, Finland*

K.-A. Suominen*
*Research Institute for Theoretical Physics, University of Helsinki, P.O. Box 9, FIN-00014 Helsinki, Finland*
(Received 20 December 1993)

We present analytical predictions based on a semiclassical theory concerning a single-mode cw laser interaction with longitudinally Zeeman tuned $J = 1 - J = 0$ atomic systems. In the theoretical model, the laser frequency detuning from the inhomogeneously broadened absorber line center is considered. Equations for the interaction signal are derived for all rotations of a polarizing analyzer transmission axis with respect to an original laser beam linear polarization. Results are presented for the forward-scattering case when the analyzer transmission axis is orthogonal to the beam polarization. Calculated results on bright and dark ring-shaped light structures are compared with experimental ones originating from a Gaussian beam interaction with a neon $1s_4(J = 1,\ g = 1.464) - 2p_3(J = 0)$ transition. Calculated results on forward-scattering spectra are presented, i.e., the forward-scattering light intensity as a function of the longitudinal magnetic tuning when the laser frequency is fixed to selected detunings from the absorber line center. Spectra are presented both for the case when the inhomogeneously broadened line originates from a single absorbing isotope and for the case when it originates from overlapping contributions of two isotopes. The results show that laser frequency detunings of tens of megahertz from the absorber line center(s) show up in the forward-scattering spectra. The conclusion is that reliable data on atomic parameters of a nonlinearly absorbing sample can be extracted from experimental spectra only when the sample is monoisotopic and when the laser frequency detuning from the absorber line center is known.

PACS number(s): 32.80.Bx, 33.55.Fi

## I. INTRODUCTION

Lately much interest has been devoted to ring structures that appear in laser light that has traversed an absorbing medium [1]. Particularly the phenomenon known as conical emission has been much investigated [2–5]. Spectacular ring structures can appear in various shapes and their origin can be different depending on the medium with which the light interacts.

Recently we have reported on investigations of ring structures that appear in a magneto-optic experiment [6]. The ring structures are observed in the forward-scattered light, the origin of which is a single-mode laser interaction with a magnetically tuned neon-gas discharge. In [6] we described how the forward-scattered light ring structures depend on the magnetic field strength and on the laser power in the case when the laser frequency is tuned to the center of the Doppler broadened absorber line. In this paper we describe how the ring structures depend on the laser frequency detuning from the absorber line center. We also describe how the detuning affects the forward-scattering spectra, i.e., the scattered light intensity as a function of the magnetic field strength.

As in conical emission [2–5] the laser frequency detuning from the absorber line center plays an important role in the features that appear in the ring structures of the forward-scattered light. The detuning also has quite a strong influence on the forward-scattering spectra. If the sample consists of more than just one isotope (in our case two neon isotopes) the frequency detuning is an important parameter in the analysis of the spectra. To explain the observable features in the ring structures and the spectra, we have carried out a semiclassical calculation where the effects of a detuned laser frequency are taken into account.

A forward-scattering experiment is one version of a level-crossing experiment. In a forward-scattering experiment only the light that has interacted with the sample is selectively detected. This is accomplished by introducing an analyzing polarizer in the light beam that has traversed a magnetically tuned sample. The transmission axis of the analyzer is crossed ($\alpha = \pi/2$) with respect to the original linear polarization of the beam. This experimental arrangement results in the detection of the dispersive contributions of the light-matter interaction. If the transmission axis of the analyzer is orientated parallel ($\alpha = 0$) with the beam polarization or if the analyzer is removed from the experiment, the detection in the traversed beam results in a signal originating from the absorptive light-matter interactions. If the analyzer is introduced with transmission axis orientations $0 < \alpha < \pi/2$, the signal consists of a mixture of the dispersive and the absorptive compo-

*Present address: Clarendon Laboratory, University of Oxford, Parks Road, Oxford OX1 3PU, United Kingdom.

 

nents [7]. We term the $\alpha \neq \pi/2$ experiments zero-field level-crossing experiments and the $\alpha = \pi/2$ experiments forward-scattering experiments, respectively. Moreover, with forward-scattered light we mean the light which has interacted and which propagates in the same direction as the primary light beam that traverses the absorber.

In a zero-field level-crossing experiment the light-matter interaction signal is embedded in the total light that has traversed the absorber. To extract the weak signal from the total light a modulation of the interaction, i.e., of the sample, is required. In magneto-optic experiments this modulation is introduced by a small amplitude (ac) magnetic field superimposed on the tuning (dc) magnetic field. Using the magnetic modulation frequency as a reference frequency for lock-in detection, the weak interaction signal can be measured. A forward-scattering experiment does not require magnetic modulation of the sample because the analyzing polarizer extracts the interaction signal from the total traversed light.

After this introductory section we very briefly describe our experiment in Sec. II. Then in Sec. III we give our theoretical derivations in a general form. The equations include predictions on both the zero-field level-crossing and the forward-scattering signal shapes. In Sec. IV we present results on the ring structures. In Sec. V we present results on the forward-scattering spectra. We close the paper with a discussion.

## II. EXPERIMENT

The experimental results presented in this paper have been obtained with exactly the same setup presented in our previous paper [6]. Therefore we give only a very brief description on the apparatus. For more detailed information we refer to [6].

Into our 9-cm-long neon-gas discharge cell we focus ($f$ = 10 cm) a single-mode ring dye laser beam. The laser is optimized to lase on a $TEM_{00}$ mode. The inner diameter of the cell is 4 mm. The useful discharge length is 4 cm and the gas consists of natural neon. Ordinarily we use gas pressures from 50 Pa to 100 Pa (0.4–0.8 Torr) and dc discharge currents from 5 mA to 10 mA. At the entrance of the cell a linear polarization of the beam is ensured with a polarizer. A crossed polarizer serves as an analyzer for the outgoing beam. A longitudinal magnetic field along the discharge is derived from a pair of Helmholtz coils. The forward-scattered laser light is detected (depending on the measurements) either by a 1728-pixel linear charge coupled device (CCD) or an ordinary $p$-$i$-$n$ photodiode.

In our previous work [6] we investigated the forward-scattered transverse intensity distribution and the spectra when the laser frequency was tuned to the maximum absorption frequency of the selected Doppler broadened neon transition. Now we investigate how the distribution and the spectra are affected when the laser frequency is detuned from the Doppler broadened line center. Performing the experiments we start with the laser frequency corresponding to the maximum absorption and then we detune the frequency of our dye laser (CR-699-21) in intervals of the order of 100 MHz. As the gas in our discharge cell consists of natural neon (91% of $^{20}$Ne and 9% of $^{22}$Ne), the frequency corresponding to the maximum absorption is not exactly the Doppler line center frequency of the $1s_4(J = 1, g = 1.464) - 2p_3(J = 0)^{20}$Ne transition. The maximum absorption frequency is slightly above the $^{20}$Ne line center frequency.

The experimental results that are compared with the theoretical ones in Sec. IV are derived as follows. Using the CCD equipment we have recorded the forward-scattered transverse intensity distributions. This has been done after fixing the laser frequency and the longitudinal magnetic field strength to preselected values.

## III. THEORY

In our former studies of zero-field level crossings [7] and forward-scattering [6] we have considered the case where the optical frequency $\Omega$ of the interacting laser was tuned to the line center $\omega_0$ of a Doppler broadened atomic transition. Now we extend our theoretical treatment to include a laser detuning $\delta$ from the line center (Fig. 1). When the laser frequency is detuned ($\delta \neq 0$) and when the sample is subjected to a longitudinal magnetic field ($B$) the interaction occurs in unequally populated distributions corresponding to the Zeeman tuned $\Delta m = +1$ and $\Delta m = -1$ sublevel transitions. This type ($\Omega \neq \omega_0$) of a magneto-optic interaction results in a new term in our final expressions for the total signal compared with the case $\Omega = \omega_0$. Our derivation for the signal is given as follows.

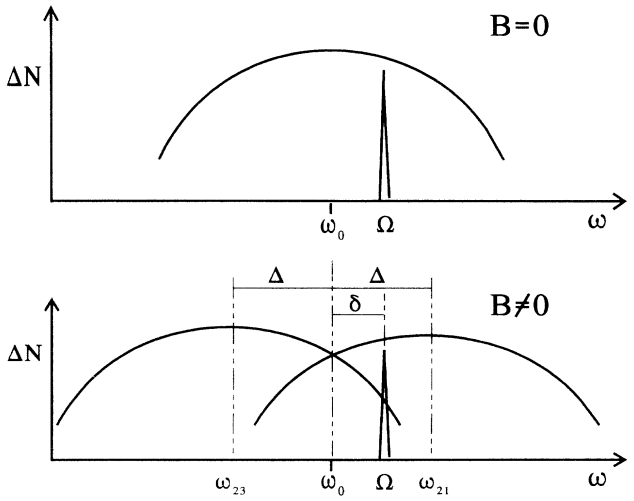


FIG. 1. Illustration of the absorption density $\Delta N$ as a function of the optical frequency $\omega$. The single-mode laser frequency $\Omega$ is detuned ($\delta$) from the absorber line center frequency $\omega_0$. The upper part shows how the laser interacts with one distribution only when no magnetic field is applied ($B = 0$). The lower part shows how the laser interacts with two distributions when a longitudinal magnetic field ($B \neq 0$) splits the absorbing $J = 1 - J = 0$ atomic systems.

The laser beam, characterized by the frequency $\Omega$ and the wave number $k$, is described as a superposition of two counterrotating circularly (+ and −) polarized fields which propagate along the $z$ axis

$$\mathbf{E}(z,t) = \boldsymbol{\mathcal{E}}(z)\exp[i(kz+\Omega t)] + \text{c.c.}, \tag{1}$$

where $\boldsymbol{\mathcal{E}}(z) = E_+(z)\mathbf{e}_+ + E_-(z)\mathbf{e}_-$ and $\mathbf{e}_+ = (\mathbf{e}_x + i\mathbf{e}_y)/\sqrt{2} = \mathbf{e}_-^*$. In the $\Lambda$-type system (Fig. 2) that we study the $\Delta m = +1$ and $\Delta m = -1$ couplings are due to the $E_+$ and $E_-$ components of the field, respectively. We work in the rotating-wave approximation limit. The field traverses the absorber and it is modified by the induced polarization $\mathbf{P}$ of the absorber gas. The polarization $\mathbf{P}$ is taken to be parallel with $\mathbf{E}$ and we write

$$\mathbf{P}(z) = \boldsymbol{\mathcal{P}}(z)\exp[-i(kz+\Omega t)] + \text{c.c.}, \tag{2}$$

where $\boldsymbol{\mathcal{P}}(z) = P_+(z)\mathbf{e}_+ + P_-(z)\mathbf{e}_-$. By substituting Eqs. (1) and (2) into the wave equation and assuming that the amplitudes in (1) and (2) are slowly varying, a relation between the amplitudes is obtained [6]. As the gas in the absorber is considered optically thin, we have $\mathbf{P}(\boldsymbol{\mathcal{E}}(z)) \simeq \mathbf{P}(\boldsymbol{\mathcal{E}}(0))$. The field out from the cell is

$$\mathbf{E}(L,t) = \mathbf{E}(0,t) + \frac{\Omega L}{c\varepsilon_0}\,\text{Im}\left\{\boldsymbol{\mathcal{P}}(0)\exp\left[-i(kz+\Omega t)\right]\right\}, \tag{3}$$

where $L$ is the length of the interacting medium. We describe the analyzer used in the measurements of the outcoming field with the unit vector $\boldsymbol{\alpha} = \boldsymbol{e}_x\cos(\alpha) + \boldsymbol{e}_y\sin(\alpha)$. The measured signal is proportional to

$$[\mathbf{E}(L,t)\cdot\boldsymbol{\alpha}]^2 = [\mathbf{E}(0,t)\cdot\boldsymbol{\alpha}]^2 + \frac{2\Omega L}{c\varepsilon_0}\,[\mathbf{E}(0,t)\cdot\boldsymbol{\alpha}]\,\text{Im}\left\{[\boldsymbol{\mathcal{P}}(0)\cdot\boldsymbol{\alpha}]\exp[-i(kz+\Omega t)]\right\} + \left(\frac{\Omega L}{c\varepsilon_0}\,\text{Im}\left\{[\boldsymbol{\mathcal{P}}(0)\cdot\boldsymbol{\alpha}]\exp[-i(kz+\Omega t)]\right\}\right)^2. \tag{4}$$

The times associated with the optical frequencies are very short compared with the measurement time constants. Time averaging gives the signal

$$\begin{aligned} S \propto\ & (\boldsymbol{\mathcal{E}}\cdot\boldsymbol{\alpha})\,(\boldsymbol{\mathcal{E}}^*\cdot\boldsymbol{\alpha}) + \kappa[\text{Im}\{(E_+ + E_-)(P_+ + P_-)\}\cos^2\alpha - \text{Im}\{(E_+ - E_-)(P_+ - P_-)\}\sin^2\alpha \\ & + 2\text{Re}\{E_+P_+ - E_-P_-\}\cos\alpha\sin\alpha] + \frac{\kappa^2}{2}[|P_+ + P_-|^2\cos^2\alpha \\ & + |P_+ - P_-|^2\sin^2\alpha + \text{Im}\{(P_+ + P_-)(P_+ - P_-)^* - (P_+ - P_-)(P_+ + P_-)^*\}\cos\alpha\sin\alpha], \end{aligned} \tag{5}$$

where $\alpha$ is the angle between the analyzer transmission axis with respect to the $x$ axis, $\kappa = \Omega L/c\varepsilon_0$, and $E_\pm, P_\pm$ are given at $z = 0$.

The polarization components

$$P_+(z)\mathbf{e}_+ + P_-(z)\mathbf{e}_-$$

$$= N[\mu\,\tilde{\rho}_{21}\,\mathbf{e}_+ + \mu\,\tilde{\rho}_{23}\,\mathbf{e}_-]\exp[i(kz+\Omega t)] + \text{c.c.} \tag{6}$$

are calculated using density matrix formalism. The parameter $N$ is the atom density factor and it includes the Gaussian velocity distribution of the atoms. The parameter $\mu$ is the dipole moment. To obtain the necessary density matrix components

$$\tilde{\rho}_{2j} \equiv \rho_{2j}\exp[-i(kz+\Omega t)] \tag{7}$$

we use perturbation expansions, which are easily derived with the diagrammatic technique (see, e.g., [8] and [9] for a description). The polarization is calculated to the third order. We consider a pure $J = 1$ to $J = 0$ transition

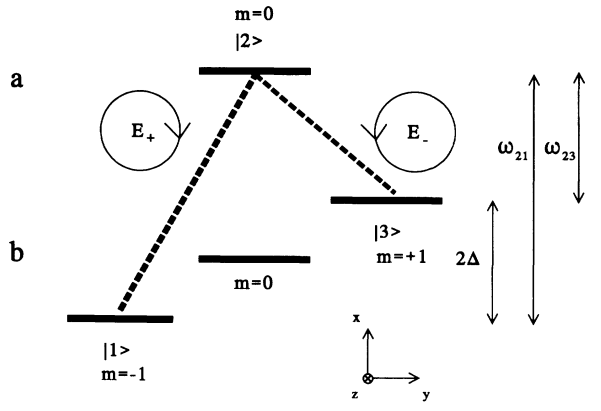


FIG. 2. Schematics of the interaction between the laser field components $E_+$ and $E_-$ with the magnetically tuned $J = 1 - J = 0$ system. The field is assumed to propagate in the $z$ direction. The magnetic splitting between the $m = \pm 1$ sublevels of the lower state $b$ is $2\Delta$ and the transition frequencies for the $|\Delta m| = 1$ selection rule between the state $a$ and $b$ are $\omega_{21}$ and $\omega_{23}$.

(Fig. 2). Unlike our earlier study [6], we now introduce a detuning $\delta$ of the laser frequency into the calculations. The detuning is defined as (see Figs. 1 and 2)

$$\delta = \Omega - \omega_{21} + \Delta = \Omega - \omega_{23} - \Delta \ , \tag{8}$$

where $\Delta = g\mu_B B/h$ is the magnetic splitting between the Zeeman sublevels. The magnetic field $\mathbf{B}$ is in the $z$ direction, $g$ is the Landé factor, $\mu_B$ is the Bohr magneton, and $h$ is Planck's constant. When the magnetic tuning is given the value $\Delta = 0$, then $\omega_{21} = \omega_{23} = \omega_0$ and Eq. (8) reduces to $\delta = \Omega - \omega_0$. The aim of the derivation that follows is to end up with an expression where the predicted signal is given explicitly as a function of the parameters $\delta$ and $\Delta$. In the case of our investigations of the forward-scattered transverse intensity distributions we give fixed values of both $\delta$ and $\Delta$. When we investigate the spectra we fix the $\delta$ value and perform the calculations as a function of $\Delta$. The first term $(\boldsymbol{\mathcal{E}} \cdot \boldsymbol{\alpha})(\boldsymbol{\mathcal{E}}^* \cdot \boldsymbol{\alpha})$ in Eq. (5) does not contain information on the light-atom interaction and it can be ignored.

We consider the incoming field to be linearly polarized, i.e., $E_+ = E_-$. Hence the term proportional to $\sin^2\alpha$ in the first set of square brackets in Eq. (5) is zero. Unless the analyzer angle $\alpha$ is $\pi/2$, the third term proportional to $\kappa^2$ is a negligible fluorescence term compared with the second term in Eq. (5) and can be neglected. Then we obtain (when the parameter $\kappa$ is omitted) the signal

$$S \propto S_1 \cos^2\alpha + S_2 \sin\alpha\cos\alpha \ , \tag{9}$$

where

$$S_1 = \beta N \,\mathrm{Im}\left\{ \tilde{\rho}_{21} + \tilde{\rho}_{23} \right\} \tag{10}$$

and

$$S_2 = \beta N \,\mathrm{Re}\left\{ \tilde{\rho}_{21} - \tilde{\rho}_{23} \right\} . \tag{11}$$

The parameter $\beta$ is the Rabi frequency ($\beta = E\mu/h$). When we take into account the transverse effects the laser beam induces we use the spatially dependent Rabi frequency

$$\beta^2(r) = \left(\frac{E_0\mu}{h}\right)^2 \exp\left[-\left(\frac{r}{r_0}\right)^2\right] , \tag{12}$$

where $r_0$ is the distance from the beam center where the intensity has decreased to $1/e$ of its maximum value $(E_0)^2$.

To derive the final expression for $S_1$ and $S_2$ using Eqs. (10) and (11), respectively, we utilize standard methods in these contexts [10]. In addition to the assumptions presented above in giving Eqs. (2), (3), (5), (6), and (7), we assume the Doppler limit approximation to hold. By combining all terms of first and second order in laser intensity ($\beta^2$) we finally obtain

$$\begin{aligned} S_1 = {} & 2\sqrt{\pi}\,\beta^2\Lambda \exp\left[-\left(\delta^2+\Delta^2\right)\right]\cosh(2\delta\Delta) \\ & \times\Bigg[1 - \beta^2\,\gamma_{ab}^{-1}\left(\gamma_a^{-1}+\gamma_{b'}^{-1}\right) \\ & -\beta^2\left(\frac{2\gamma_{ab}-\gamma_a-\gamma_b}{\gamma_a(2\gamma_{ab}-\gamma_b)}\,\frac{\gamma_{ab}}{\gamma_{ab}^2+\Delta^2}\right. \\ & \left.+\frac{2}{2\gamma_{ab}-\gamma_b}\,\frac{\gamma_b}{\gamma_b^2+4\Delta^2}\right)\Bigg] \end{aligned} \tag{13}$$

and

$$\begin{aligned} S_2 = {} & 2\sqrt{\pi}\,\beta^2\Lambda \exp\left[-\left(\delta^2+\Delta^2\right)\right] \\ & \times\left\{\left[\frac{2\Delta}{\sqrt{\pi}}\cosh(2\delta\Delta) - \frac{2\delta}{\sqrt{\pi}}\sinh(2\delta\Delta)\right]\right. \\ & -\beta^2\left[\frac{2\gamma_{ab}-\gamma_a-\gamma_b}{\gamma_a(2\gamma_{ab}-\gamma_b)}\,\frac{\Delta}{\gamma_{ab}^2+\Delta^2}\right. \\ & \left.\left.+\frac{2}{2\gamma_{ab}-\gamma_b}\,\frac{2\Delta}{\gamma_b^2+4\Delta^2}\right]\cosh(2\delta\Delta)\right\} . \end{aligned} \tag{14}$$

Because Eqs. (13) and (14) are derived in the Doppler limit, we have, for all parameters, $\gamma_a, \gamma_{b'}, \gamma_b, \gamma_{ab}, \Delta, \delta \ll 1$ when scaled with the Doppler width $ku = 1$. The parameters $\gamma_a$ and $\gamma_{b'}$ represent the population damping constant of the upper and the lower level, respectively. The parameter $\gamma_{ab}$ is the coherence damping constant between the upper and lower level whereas the parameter $\gamma_b$ is the coherence damping constant between the sublevels in the lower state. The parameter $\Lambda$ is the scaled difference of the gas discharge pumping rates of the levels $a$ and $b$.

If the analyzer transmission axis is orientated parallel to the polarization direction of the incoming laser field ($\alpha = 0$) only the term corresponding to $S_1$ in the signal remains in Eq. (9). As seen from Eqs. (10) and (13) the $S_1$ term contains information only on the absorptive light-matter interactions.

If the analyzer angle has a value $0 < \alpha < \pi/2$, the total signal [Eq. (9)] contains, in addition to $S_1$, information on the dispersive part $S_2$ [Eqs. (11) and (14)] of the light-matter interaction. In the limit of zero laser detuning ($\delta = 0$) the expressions for $S_1$ and $S_2$ [Eqs. (13) and (14)] reduce into those we have utilized in our earlier zero-field level-crossing investigations [7].

Next we consider the forward-scattering case $\alpha = \pi/2$. For this geometry the first term $(\boldsymbol{\mathcal{E}} \cdot \boldsymbol{\alpha})(\boldsymbol{\mathcal{E}}^* \cdot \boldsymbol{\alpha})$ in Eq. (5) is zero. All the terms in the first set of square brackets in Eq. (5) disappear: the first term due to the geometry, the second term due to the linear polarization of the laser beam, and the third term due to the geometry. Only one term ($|P_+ - P_-|^2 \sin^2\alpha$) in the second set of square brackets remains in Eq. (5). Calculations with the same assumptions presented above give the signal

$$S \propto \frac{\kappa^2}{\beta}\left(S_2^2 + S_3^2\right) , \tag{15}$$

where $S_2$ is given by Eq. (14). The new signal factor $S_3$ derives from the detuned laser frequency. It is [compare with Eqs. (10) and (11)]

$$S_3 = -\beta N \,\mathrm{Im}\left\{ \tilde{\rho}_{21} - \tilde{\rho}_{23} \right\} . \tag{16}$$

The final expression is

$$S_3 = 2\sqrt{\pi}\,\beta^2 \Lambda \exp\left[-\left(\delta^2 + \Delta^2\right)\right] \sinh\left(2\delta\Delta\right) \times \left[1 - \beta^2 \gamma_{ab}^{-1}\left(\gamma_a^{-1} - \gamma_b^{-1}\right)\right] , \tag{17}$$

which is very similar to the first part of $S_1$ [Eq. (13)]. One should note that this signal contribution ($S_3$) disappears as the laser detuning $\delta$ goes to zero, justifying the forward-scattering expression $[\mathrm{Im}(\boldsymbol{\mathcal{P}} \cdot \boldsymbol{\alpha})]^2$ that we have used in our earlier studies [6].

## IV. RESULTS ON TRANSVERSE LIGHT INTENSITY DISTRIBUTIONS

In this section we present both experimental and calculated results. We show how the transverse intensity distribution of forward-scattered light depends on the laser frequency detuning when the magnetic field strength is fixed to a preselected value.

In Fig. 3 we show experimental results. The forward-scattered light intensity is shown as a function of the position on the CCD. The recordings have been obtained using the $1s_4(J = 1, g = 1.464) - 2p_3(J = 0)$ transition in neon. The corresponding laser wavelength is 607.4 nm. All the curves shown in Fig. 3 have been recorded with the gas pressure 75 Pa (0.56 Torr), the discharge current 6 mA, the laser input power 10 mW, and the magnetic field tuning $\Delta = g\mu_B B/h = 156$ MHz. The laser detuning value $\delta = 0$ MHz corresponds to the maximum absorption of the laser beam when the magnetic field is not applied ($\Delta = 0$ MHz). For the fixed magnetic tuning value $\Delta = 156$ MHz (used in recording the curves of Fig. 3) the 10-mW laser input power induces a total forward-scattered light power of 10 $\mu$W in the $\delta = 0$ MHz case. With the recordings above the lowest one we show how the transverse distribution of the light changes when the laser frequency is tuned to higher frequencies from the value used in recording the lowest curve. The areas of the distributions are proportional to the scattered light power and all results in Fig. 3 are directly comparable with each other. Obviously, when the laser detuning from the line center is large, as in the case of the uppermost curve (600 MHz) in Fig. 3, the ring structures in the scattered light disappear and the intensity (or the power) of the light becomes higher than in the case of smaller laser detunings.

To obtain a calculated reproduction of the curves presented in Fig. 3 we have used Eqs. (12), (14), (15), and (17). The results are plotted in Fig. 4. For the decay parameters (in frequency units) we have used $\gamma_a = 10$ MHz, $\gamma_b = 30$ MHz, and $\gamma_{ab} = 84$ MHz. For the Rabi frequency we have used $\beta^2 = 0.45$ (MHz)$^2$. The

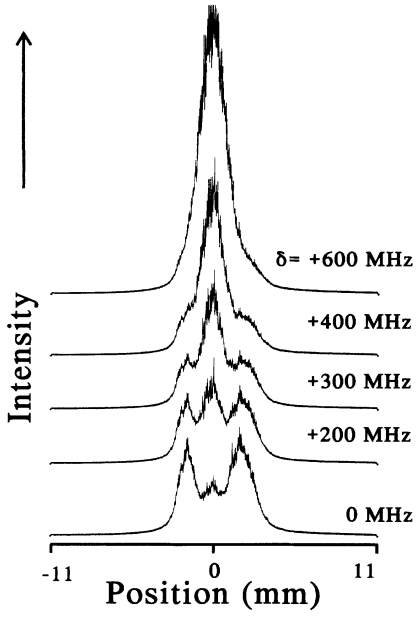


FIG. 3. Experimental forward-scattering light intensity as a function of the position on the CCD. Neon transition: $1s_4(J = 1, g = 1.464) - 2p_3(J = 0)$. The laser frequency detuning from the maximum absorption frequency, i.e., the parameter $\delta$, starts with $\delta = 0$ MHz and ends with $\delta = +600$ MHz. All the recordings have been obtained with the gas pressure 75 Pa, the discharge current 6 mA, and the fixed magnetic tuning $\Delta = 156$ MHz. The laser input power was 10 mW, which gave, in the lowest case ($\delta = 0$ MHz), a total forward-scattered light power of 10 $\mu$W.

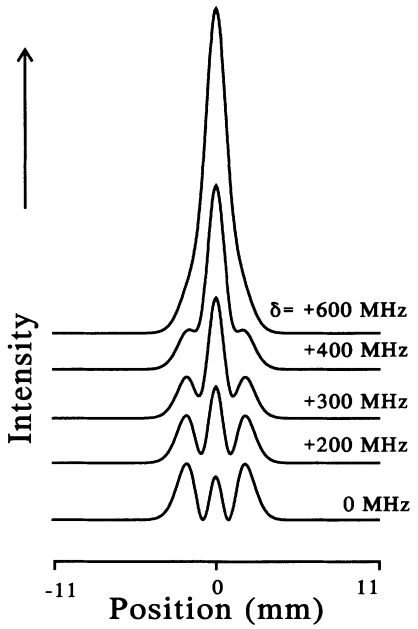


FIG. 4. Calculated results on the transverse intensity distribution of forward-scattered light to be compared with the curves of Fig. 3. These curves have been calculated using Eqs. (12), (14), (15), and (17).

beam radius has been extracted from a least-squares fit of a Gaussian distribution to an experimentally recorded beam profile in order to perform the spatial integration over the transverse direction (for details see [6]). In the calculations of the curves in Fig. 4 we have assumed that the laser interacts with one Gaussian shaped absorptive profile only (compare with Sec. V). Analogously to our previous studies [6] we have not tried to carry out detailed fit procedures of our theoretical expressions to the experimental data. We have only inserted realistic parameter values into our equations to examine if the relevant features of the experimental curves can theoretically be reproduced. The intensity scale in Fig. 4 is the same for all curves, i.e., the curves are directly comparable with each other. We should point out that the term $S_3$, Eq. (17), becomes more important when the laser frequency detuning is increased. For the detunings 400 MHz and 600 MHz the calculated curves do not show the same wing structures as the experimental ones if the term $S_3$ is omitted.

An explanation for the physical processes which cause the ring structures can be given with the information provided by Eqs. (12), (14), (15), and (17). Let us first assume that the laser detuning is small ($\delta \approx 0$) so the $S_3$ contribution of Eq. (17) can be ignored. The expression for $S_2$ [Eq. (14)] consists of two parts, one proportional to $\beta^2(r)$ and the other proportional to $\beta^4(r)$. For small $\delta$'s these two parts have opposite signs. Let us further assume that the laser power is at a constant level where the nonlinear $\beta^4(r)$ contributions in $S_2$ are significant. The atoms interacting with the very center areas of the beam experience a stronger field than the ones in the wings of the beam transverse intensity distribution. For small magnetic tunings ($\Delta$), the nonlinear $\beta^4(r)$ contributions in $S_2$ are dominant. When the magnetic tuning $\Delta$ is increased, the linear part proportional to $\beta^2(r)$ becomes comparable with the nonlinear part proportional to $\beta^4(r)$. For some value of $\beta(r)$, the linear and the nonlinear contributions will cancel and cause a dip in the transverse intensity distribution. Because the laser intensity has a Gaussian transverse dependence, the cancellation occurs for different magnetic tunings $\Delta$ for the interaction in the center and in the wings of the intensity distribution. If the magnetic tuning $\Delta$ is made large, the nonlinear contributions are driven out of the interaction and the linear part remains.

Let us now fix the magnetic tuning $\Delta$ to a value where a dip in the center of the forward-scattered light intensity is observed. This corresponds approximately to the case shown by the lowest $\delta = 0$ MHz curve in Figs. 3 and 4. When the laser detuning $\delta$ is increased ($\delta > 0$), the proportions with which the linear [$\beta^2(r)$] and the nonlinear [$\beta^4(r)$] parts in $S_2$ [Eq. (14)] contribute are changed. The contribution from $S_3$ [Eq. (17)] is increased with increasing $\delta$. When $\delta$ is further increased and $\Delta$ is kept fixed, the linear $\beta^2(r)$ contribution term $-(2\delta/\sqrt{\pi})\sinh(2\delta\Delta)$ becomes larger than the term $(2\Delta/\sqrt{\pi})\cosh(2\delta\Delta)$. Thus the linear $\beta^2(r)$ contribution gets the same (−) sign as the nonlinear $\beta^4(r)$ contribution. This results in a strong growth of the forward-scattered light intensity (see Figs. 3 and 4).

## V. CONSEQUENCES TO SPECTRA OF FORWARD-SCATTERED LIGHT

In forward-scattering experiments information about the light-matter interactions is usually derived from the measurements of the scattered light intensity as a function of the magnetic tuning of the sample. Our previous paper [6] dealt with the consequences of the laser beam transverse intensity distribution to forward-scattering spectra. Now we present results on how the spectra depend on the laser frequency.

It has already been mentioned that we perform our experiments with natural neon gas. Natural neon consists of 91% of $^{20}$Ne, 9% of $^{22}$Ne, and a vanishing amount of $^{21}$Ne. The isotope shifts (1–3 GHz) [11–14] between the $^{20}$Ne and $^{22}$Ne transitions are nearly the same as the Doppler broadened transition full half-widths $\nu_D = (2\sqrt{\ln 2})ku \approx 1.5$ GHz. Thus, strictly taken, the neon absorber line consists of two overlapping contributions. Depending on the absolute optical frequency of the laser, the interaction with both contributions may or may not be relevant. If the laser frequency is tuned to the center of the $^{20}$Ne isotope line, the contribution to the signal from the $^{22}$Ne isotope is weak because of its relatively small amount in natural neon. Detuning of the laser to higher frequencies from that of the $^{20}$Ne line center frequency increases the $^{22}$Ne contribution. If the laser is tuned to $^{22}$Ne line center frequency, the contribution from the $^{20}$Ne is still quite remarkable because of its large amount in natural neon.

To tune experimentally a single-mode laser exactly to a transition line center of one of the isotopes in natural neon gas, requires more sophisticated methods than monitoring of the traversed beam intensity when the laser frequency is scanned through the two overlapping absorber lines. For example, by utilizing a reference absorber, it would be possible to lock a laser to an inverted Lamb dip, the origin of which would be the interaction with one of the isotopes. Then the isotopic contribution from the other neon isotope could, in principle, be estimated in a forward-scattering experiment performed in another absorber. On the other hand, it is well known that experimental spectra obtained using lasers do not necessarily give the correct isotopic abundances of a sample [11–18]. These spectra are nonlinear; they are very sensitive to the saturation conditions in the sample. Many parameters are involved in these conditions, such as, for instance, the beam transverse profiles, the laser (de)focusing, and the radiation trapping effects.

In the following we present only calculated forward-scattering spectra due to the experimental complications discussed above. An intuitive explanation for the processes which cause the spectra is given at the end of Sec. IV. First we show how the spectra depend on the laser frequency in the case when the sample consists of just one isotope. Then we show the spectral features in the case when the sample consists of two isotopes. In both cases we do not include any assumptions about the beam transverse intensity distribution.

In Fig. 5 we show three curves corresponding to three fixed laser detunings ($\delta$) in the case of a single absorbing

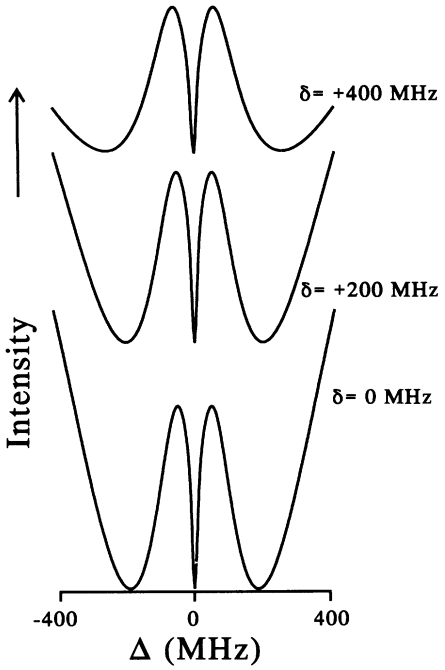


FIG. 5. Calculated forward-scattering spectra in the case of one absorbing line. The laser detunings from the line center are $\delta = 0$ MHz, $\delta = +200$ MHz, and $\delta = +400$ MHz. The curves have been calculated using Eqs. (14), (15), and (17).

line. The curves have been calculated using Eqs. (14), (15), and (17). The intensity scale (arbitrary units) is the same for all three curves in Fig. 5 so they are directly comparable with each other. For the relaxation parameters we have used $\gamma_a = 10$ MHz, $\gamma_b = 30$ MHz, and $\gamma_{ab} = 84$ MHz and for the Rabi frequency $\beta^2 = 0.45$ $(\text{MHz})^2$. The curve lowest in Fig. 5 has been calculated with the laser detuning $\delta = 0$. In this ($\delta = 0$) case the two side minima (on each side of the magnetic tuning value $\Delta = 0$) extend down to the same zero intensity value as the center ($\Delta = 0$) minimum. When the laser frequency detuning parameter is increased to $\delta = +200$ MHz and to $\delta = +400$ MHz, the side minima are lifted above the center minimum value. This feature in Fig. 5 is not as obvious as the side minima shift to larger magnetic tuning $\Delta$ values when the laser frequency detuning $\delta$ value is increased.

In Fig. 6 we show two curves corresponding to fixed laser detunings in the case of two overlapping absorber lines. The intensity (arbitrary units) scale is the same for both curves in Fig. 6 so they are directly comparable with each other. The selection of the parameters in calculation of the curves has been made so that it approximately corresponds to cases in natural neon. The center frequency separation between the two Gaussian shaped distributions is 900 MHz. The absorption density of the distribution at the higher optical frequency is assumed to be one-tenth of that at the lower optical frequency. This corresponds roughly to 91% $^{20}$Ne and 9% $^{22}$Ne. The contribution from the two distributions to the intensity of the forward-scattered light is assumed to be linearly proportional to the number density of the absorbing atoms in the velocity group with which the laser is interacting. No assumptions on different saturation strengths in the two ensembles have been made. For both ensembles we have used the same relaxation and Rabi frequency values as before [$\gamma_a = 10$ MHz, $\gamma_b = 30$ MHz, $\gamma_{ab} = 84$ MHz, and $\beta^2 = 0.45$ $(\text{MHz})^2$]. For the Doppler full linewidths we have used the value $\nu_D = 1400$ MHz for both ensembles. The calculations of curves in Fig. 6 have been done using Eqs. (14), (15), and (17).

The upper curve in Fig. 6 shows the forward-scattering spectrum when the laser frequency is tuned to the center ($\delta_1 = 0$ MHz) of the ($^{20}$Ne) line at the lower frequency. This selection of the laser frequency gives automatically the detuning $\delta_2 = -900$ MHz from the line center of the ($^{22}$Ne) distribution at the higher frequency ($\delta_2 = \delta_1 - 900$ MHz). At the detuning frequency $\delta_2 = -900$ MHz the contribution to the total signal from the higher frequency distribution is quite small. Still, as can be seen from the upper curve in Fig. 6, this contribution is readily observable. The side minima of the curve are clearly above the center ($\Delta = 0$) minimum zero value.

When the laser frequency is detuned from the line cen-

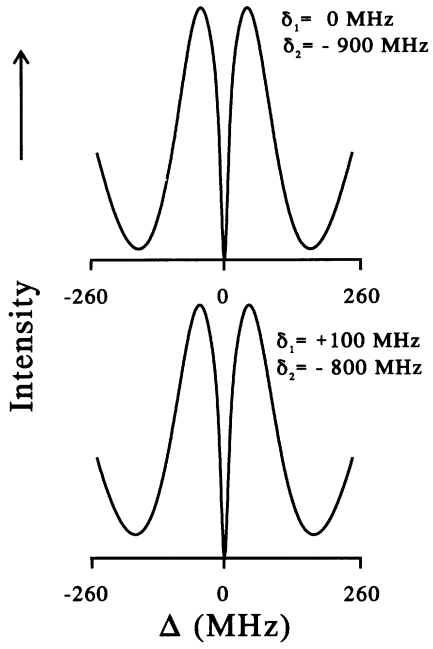


FIG. 6. Calculated forward-scattering spectra in the case of two overlapping absorber lines. The separation (i.e., the isotope shift) of the lines is taken to be 900 MHz. The absorption density of the line at the higher frequency is taken to be one-tenth of that of the one at the lower frequency. The upper curve has been calculated when the laser frequency is assumed to be at the center ($\delta_1 = 0$ MHz) of the line at the lower frequency giving a detuning $\delta_2 = -900$ MHz from the center of the line at the higher frequency. The lower curve shows the spectrum when the laser is detuned from both line centers ($\delta_1 = +100$ MHz and $\delta_2 = -800$ MHz). The curves have been calculated using Eqs. (14), (15), and (17).

ters of both distributions the side minima always rise above the minimum value they take when the frequency is tuned to the line center of the dominant distribution. This is illustrated with the lower curve in Fig. 6. The detuning from the dominant ($^{20}$Ne) distribution line center is $\delta_1 = +100$ MHz, corresponding to the detuning $\delta_2 = -800$ MHz from the higher frequency ($^{22}$Ne) distribution line center. Compared with the upper curve of Fig. 6, the lower curve shows two times higher side minima deviations from the center ($\Delta = 0$) minimum value than the upper one.

The curves shown in Figs. 5 and 6 were obtained by keeping the laser detunings $\delta$ fixed at preselected values and by plotting the forward-scattered light intensity as a function of the magnetic tuning $\Delta$. Next we present curves where we keep the magnetic tuning fixed and plot the light intensity as a function of the laser detuning. In Fig. 7 we show the forward-scattered light intensity dependence on the laser frequency detuning $\delta_1$ from the center of the dominant $^{20}$Ne absorber line. The curves in Fig. 7 have been calculated using Eqs. (14), (15), and (17). The intensity scale is in arbitrary units and it is the same for all curves in Fig. 7. The curve positions and magnitudes are those obtained directly from the calculation. A careful examination of the curves shows that they are slightly asymmetric with respect to the $\delta_1 = 0$ value. These asymmetries originate from the 10% abundance of the $^{22}$Ne isotope in the absorber. The parameter values used in the calculations of the curves are the same as before. As seen from Fig. 7, the signal dependence on the laser frequency detuning is quite strong. A conclusion that can be made from the curves of Fig. 7 is that forward scattering should be applicable to laser stabilization. By fixing the magnetic field strength to a value $\Delta > 0$ it should be possible to frequency lock a laser on detunings well below or above the value $\delta_1 = 0$.

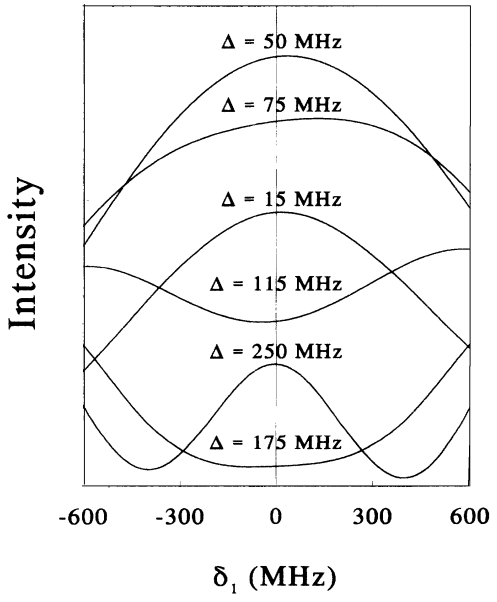


FIG. 7. Calculated results on forward-scattering light intensity as a function of the laser frequency detuning parameter $\delta_1$ in the case of two overlapping absorber lines (see the text of Fig. 6). The curves have been calculated [using Eqs. (14), (15), and (17)] for the fixed magnetic tunings $\Delta$ as given.

## VI. DISCUSSION

We have investigated nonlinear forward-scattering effects as a function of the interacting laser optical frequency. We have investigated both the forward-scattered light transverse intensity distributions and the forward-scattering spectra when the laser frequency is detuned from the absorber Doppler line center. In our studies we have not tried to perform detailed fit procedures of our theoretical expressions to experimental data. Rather we have considered one case at the time, i.e., we have introduced one variable at the time to show how it affects the forward-scattering signals.

In the theoretical part of this work we have presented expressions for both zero-field level-crossing and forward-scattering signals. Comparing the calculated results in this work with those of our previous work [6,7] we conclude that in the forward-scattering case [Eq. (15)] we obtain a new term ($S_3$) in the signal expression when the laser is detuned from the line center. In the zero-field level-crossing case the terms [$S_1$ and $S_2$, Eqs. (13) and (14)] include detuning contributions that do not show up as significantly as they do in the forward-scattering case.

Zero-field level-crossing experiments can be carried out placing a detector directly in the beam that has traversed a sample. Looking at Eq. (5) it can be concluded that by introducing an analyzing polarizer in the experiment considerable signal-to-noise improvement can be obtained. The first term $(\boldsymbol{\mathcal{E}} \cdot \boldsymbol{\alpha})(\boldsymbol{\mathcal{E}}^* \cdot \boldsymbol{\alpha})$ in Eq. (5) does not contain information on the light-matter interaction. The dazzling effect of the laser beam that has traversed the sample is much reduced when the analyzer is inserted at $\alpha \neq 0$ angles. The most favorable experimental conditions are obtained for $\alpha = \pi/2$, i.e., only the forward-scattered light, "the light that has interacted" is detected. The ring structures presented in [6] and in this work can be observed clearly in the forward-scattering experimental regime only.

The results in this work and in that of our previous work [6] show that extreme care should be applied in the analysis of forward-scattering spectra. Several parameters can affect the spectra in the same way. As shown in [6], the transverse intensity distribution of the interacting beam introduces a rise of the side minima in the spectra. As shown in this work the same features in the spectra can be introduced by tuning the laser frequency away from the absorber line center. It is also shown in this work that the side minima always move upward if the sample consists of two isotopes, the Doppler broadened lines of which overlap. Both positive and negative detunings from the line center rise the side minima. In forward-scattering experiments the laser beam spatial and detuning effects as well as sample isotopic effects can simultaneously be present.

Considering the magnitude of the laser frequency detunings from the absorber Doppler line center, we conclude that already for values of tens of megahertz the detuning effects can be observed in forward-scattering spectra. The influence of such relatively small detuning does not show up as clearly in the transverse intensity distribution of the scattered light as in the spectra. Detunings of the order of hundreds of megahertz are clearly observed in the scattered light ring structures. Still, compared with detunings used in the production of conical emission [1–5], our detunings are modest. A clear difference between our forward-scattering ring structures and those of conical emission is that in our structures we do not observe generation of new frequencies [6] as they do in the conical emission structures. We want to emphasize that, although the appearance of the ring structures in forward scattering may resemble that of conical emission, the fundamental physical processes are not as extensive as those of conical emission. The ring structures in forward scattering originate from the nonlinear laser-matter interaction. Because the laser beam has a spatial intensity dependence the interaction also has a spatial dependence which shows up as ring structures in the forward-scattered light when the atoms are tuned magnetically. The physical processes discussed in explanations of conical emission are, for instance, nonresonant stimulated Raman scattering, coupling between the initial field and a transient nonlinear response of the atomic system, stimulated Raman scattering and self-phase-modulation, pulse breakup into solitary waves, the Čerenkov effect, and four-wave mixing ( [1–5] and the references therein).

## ACKNOWLEDGMENT

We are grateful to Peter Jungner for his contribution in performing the experiments.

[1] J. Opt. Soc. Am. B **7** (1990), special issue on transverse effects in nonlinear-optical systems.
[2] W. Chalupczak, W. Gawlik, and J. Zachorowski, Opt. Commun. **99**, 49 (1993).
[3] L. You, J. Mostowski, and J. Cooper, Phys. Rev. A **46**, 2903 (1992); **46**, 2925 (1992).
[4] J. F. Valley, G. Khitrova, H. M. Gibbs, J. W. Grantham, and Xu Jiajin, Phys. Rev. Lett. **64**, 2362 (1990).
[5] D. J. Harter and R. W. Boyd, Phys. Rev. A **29**, 739 (1984).
[6] P. Jungner, Å. Lindberg, and B. Ståhlberg, Phys. Rev. A **48**, 1369 (1993).
[7] P. Jungner, B. Ståhlberg, and M. Lindberg, Phys. Scr. **38**, 550 (1988).
[8] P. Jungner, B. Ståhlberg, and S. Stenholm, Opt. Commun. **72**, 345 (1989).
[9] R. Trebino, Phys. Rev. A **38**, 2921 (1988).
[10] M. Sargent III, M. O. Scully, and W. E. Lamb, Jr., *Laser Physics* (Addison-Wesley, London, 1974).
[11] B. Ståhlberg, P. Jungner, and T. Fellman, Appl. Spectrosc. **43**, 654 (1989).
[12] E. Konz, T. Kraft, and H.-G. Rubahn, Appl. Opt. **31**, 4995 (1992).
[13] F. Biraben, E. Giacobino, and G. Grynberg, Phys. Rev. A **12**, 2444 (1975).
[14] Ch. Belfrage, P. Grafström, S. Kröll, and S. Svanberg, Phys. Scr. **27**, 367 (1983).
[15] C. Delsart and J.-C. Keller, Opt. Commun. **15**, 91 (1975).
[16] C. Delsart and J.-C. Keller, Opt. Commun. **15**, 388 (1976).
[17] T. W. Hänsch, D. R. Lyons, A. L. Schawlow, A. Siegel, Z-Y. Wang, and G-Y. Yan, Opt. Commun. **38**, 47 (1981).
[18] B. Ståhlberg, P. Jungner, and T. Fellman, Opt. Commun. **70**, 329 (1989).